SAND2013-4341C

Unsteady Shock Motion in a Transonic Flow over a Wall-Mounted Hemisphere

Steven J. Beresh,[*] John F. Henfling,[†] Russell W. Spillers,[‡], and Brian O. M. Pruett[§]
Sandia National Laboratories, Albuquerque, NM, 87185

Particle image velocimetry measurements have been conducted for a Mach 0.8 flow over a wall-mounted hemisphere. The flow is strongly separated, with a mean recirculation length exceeding 5 δ and a mean reverse velocity of -0.2 U_∞. The shock foot was found to typically sit just forward of the apex of the hemisphere and move within a range of about ±10 deg. Conditional averages based upon the shock foot location show that the separation shock is positioned upstream along the hemisphere surface when reverse velocities in the recirculation region are strong and is located downstream when they are weaker. The recirculation region appears smaller when the shock is located farther downstream. No correlation was detected of the incoming boundary layer with the shock position, nor with the wake recirculation velocities. These observations are consistent with recent studies concluding that for large strong separation regions, the dominant mechanism is the instability of the separated flow rather than a direct influence of the incoming boundary layer.

Introduction

Many aircraft employ protuberances or blisters based on hemispherical geometries to house optical sensors, laser beams, electronics pods, or airborne telescopes. Unfortunately, once the flight velocity reaches the transonic range, a shock wave will form near the upper surface of such turrets, leading to massive flow separation and a highly turbulent wake. This creates aero-optical distortions that alter the propagation and distortion of any light transmitted or collected by apparatus within the turret. Moreover, the turbulence in the wake and the incoming boundary layer from the aircraft surface will induce unsteady motion to the shock wave and compound the aero-optical distortions. As a result, considerable effort is required towards the design of turret geometries that can minimize the aero-optical effects of unsteady shock motion and highly turbulent wakes.

Owing to these applications, the flow over transonic turrets has been the subject of a number of studies, with primary attention paid to the separated region responsible for most aero-optical distortion [1]. The unsteady effects of shock motion over hemispherical geometries are known but have received little attention. Instead, inferences are easily drawn from other geometries, as unsteady shock motion resulting from aircraft protuberances is a well-studied problem. It can be found in any compressible regime ranging from transonic to hypersonic and occurs on fins, ramps, cylinders, or bumps; or it may be induced by incident shocks; or simply due to the formation of a shock over curved walls. Even reviews of this phenomenon are plentiful, where articles by Smits and Dussauge [2], Dolling [3], Delery [4], and Knight et al [5] all serve as a good source of fundamental information. Recently, Clemens and Narayanaswamy [6] has reviewed the physical sources of the unsteady shock behavior in a variety of these flows. Excepting Delery [4], these reviews all are chiefly focused on supersonic shock/boundary-layer interactions; the related subject of shock motion over a transonic airfoil is reviewed by Lee [7], but in this configuration the shock motion is subject to additional influences.

Studies of unsteady shock motion over hemispheres, however, appear largely absent from the literature,

[*]Principal Member of the Technical Staff, Engineering Sciences Center, Associate Fellow AIAA, correspondence to: P.O. Box 5800, Mailstop 0825, (505) 844-4618, email: sjberes@sandia.gov
[†]Distinguished Technologist, Member AIAA
[‡]Principal Technologist
[§]Senior Technologist

This work is supported by Sandia National Laboratories and the United States Department of Energy. Sandia is a multiprogram laboratory operated by Sandia Corporation, a Lockheed Martin Company, for the United States Department of Energy's National Nuclear Security Administration under Contract DE-AC04-94AL85000.

although the closely related geometry of rounded bumps has been the subject of some investigation [8-15]. With the exception of [14], these investigations all concerned two-dimensional bumps, a noteworthy difference from the three-dimensionality of hemispherical geometries. Recent investigations by Reid et al [16] and Fang et al [17] have noted the unsteadiness of the shock over a hemisphere, but provide little data on the nature of its motion. Other experiments have directly measured the aero-optical distortion resulting from the turbulent wake [18-20], despite remaining below Mach numbers at which shocks would be generated. Though efforts at flow control over turrets have not focused on the unsteady shock behavior, they do provide some knowledge of the turbulent wake in both its natural state and forced [21-23], but again, the shock motion is not present.

The current investigation studies the flow over a wall-mounted hemisphere in a subsonic compressible flow to provide a baseline example of shock motion over a turret. Data are provided using stereoscopic Particle Image Velocimetry (PIV) to record the turbulent structure of the wake. The velocity field additionally identifies the instantaneous location of the shock wave and can be used to ascertain characteristics of its unsteady motion. The source of the shock motion may identifiable based on correlations between the shock position and flow properties in both the separated wake and the incoming boundary layer. These results contribute a new case to the existing body of literature concerning shock/boundary layer interactions, focusing on the behavior and origin of unsteady shock motion in transonic flows with a strongly turbulent separated wake.

Experimental Apparatus

Trisonic Wind Tunnel

Experiments were performed in Sandia's Trisonic Wind Tunnel (TWT), which is a blowdown-to-atmosphere facility using air as the test gas through a 305 × 305 mm^2 (12 × 12 inch^2) rectangular test section enclosed within a pressurized plenum. In its transonic configuration, several test section configurations are possible using either porous walls to alleviate the transonic choking condition or solid walls for subsonic compressible conditions. The solid-wall transonic test section was used for the present work rather than the traditional ventilated version because it offers reasonable optical access, a flat plate upon which models may be mounted from the wall, and computationally tractable boundary conditions for comparison of experimental data and numerical simulations. The use of a solid-wall test section limits the freestream Mach number of the flowfield to about 0.9.

Data given herein were acquired at a nominal freestream Mach number M_∞=0.8 with a wind tunnel stagnation pressure P_0 of 141 kPa (20.5 psia), yielding a Reynolds number based on the hemisphere radius of 630,000. The wall pressure p_w at the position of the leading edge of the hemisphere was measured using a static pressure tap in the side wall. M_∞ and the freestream velocity U_∞ were calculated isentropically from the ratio p_w/P_0 and the stagnation temperature T_0. The freestream Mach number rises with downstream distance due to boundary layer growth on the wind tunnel walls in the constant-area cross-section, but the measurement region is relatively short and the Mach number changes by less than 0.01 over this length. The wind tunnel stagnation temperature T_0 is fixed at 321K ± 2K by heating in the storage tanks, and the wall temperature is effectively constant at ambient conditions, T_w=307K ± 3K, though T_w tends to drift upward within this range as the wall warms during the course of a day.

The 99%-velocity boundary layer thickness has been measured as 13.4 ± 0.4 mm (0.53 ± 0.02 inch) from PIV data acquired in the streamwise plane on the wind tunnel centerline at about the same downstream position as the hemisphere.

Hemisphere Model

The hemisphere had a radius (and hence height) of 38.0 mm (1.495 in) and was mounted on the top wall of the wind tunnel. It was fabricated from polished acrylic to minimize the flare of the laser sheet striking it and allow measurements near the hemisphere surface. The wall upon which it mounted was made of anodized aluminum and exhibited considerably greater laser flare, which limited measurements near the wall. Since laser light entering the transparent hemisphere created an intense glow due to internal reflection, which tended to create blooming on the PIV cameras, the hemisphere was painted black except along a centerline strip where the laser sheet impinged it. A photograph of the

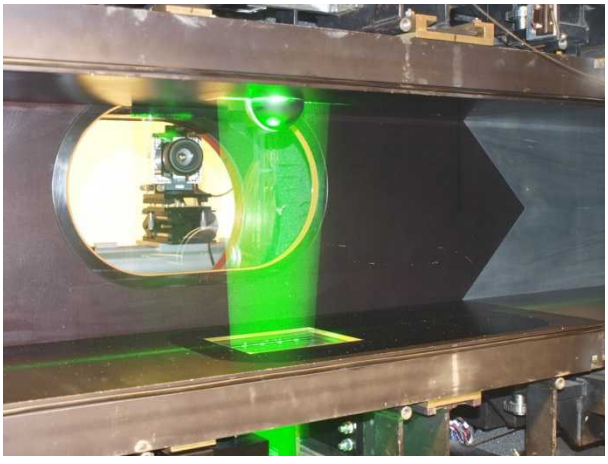

Fig. 1: Photograph of the acrylic hemisphere mounted in the wind tunnel with the laser sheet.

hemisphere mounted into the wind tunnel is given in Fig. 1, with the laser sheet visible.

Particle Image Velocimetry System

The TWT is seeded by a thermal smoke generator (Corona Vi-Count 5000) that produces a large quantity of particles typically 0.2 - 0.3 μm in diameter from a mineral oil base. Particles are delivered to the TWT's stagnation chamber upstream of the flow conditioning section through a series of pipes and tubes, in which agglomeration of the particles occurs. Previous measurement of the *in-situ* particle response across a shock wave generated by a wedge shows the particle size to be 0.7 - 0.8 μm, which holds for measurements in the transonic test section as well. Stokes numbers have been estimated as 0.04 based on *a posteriori* measurements of the hemisphere wake, which is sufficiently small to rapidly attain the local velocity even in the presence of the strongest velocity gradients in the wake.

Two separate experiments were conducted. The light source for both was a frequency-doubled dual-cavity Nd:YAG laser (Spectra Physics PIV-400) that produced about 400 mJ per beam. The beams were formed into coplanar sheets, directed into the test section from beneath the wind tunnel, and aligned to the spanwise center of the hemisphere. The laser sheet thickness was 1.2 mm, and the time between pulses was 2.70 μs in the first experiment and 1.20 μs in the second.

The two experiments were distinguished by different cameras and imaging configurations. In the first experiment, scattered laser light was collected by interline-transfer CCD cameras (Redlake MegaPlus ES4.0/E) with a resolution of 2048 × 2048 pixels digitized at 8 bits. The two cameras were equipped with 200-mm lenses mounted on Scheimpflug platforms to create an oblique focal plane aligned with the laser sheet. Stereoscopic camera calibrations were accomplished by placing a single-plane alignment target in the position of the laser sheet, then scanning it through the volume of the laser sheet to acquire seven planes of calibration data, which were calibrated using a polynomial fit. The field of view was concentrated on the top surface of the hemisphere and its wake, without data acquisition of the incoming boundary layer and leading edge of the hemisphere. A larger field of view would have compromised the spatial resolution. Images were interrogated using LaVision's DaVis v7.2 with an initial pass using 64 × 64 pixel interrogation windows, followed by two iterations of 32 × 32 pixel interrogation windows. A 50% overlap in the interrogation windows was used as well to oversample the velocity fields. The resulting vector fields were validated based upon signal-to-noise ratio, nearest-neighbor comparisons, and allowable velocity range.

In a subsequent experiment, the cameras were replaced by modern CMOS versions incorporating a double-frame mode (LaVision Imager sCMOS) with resolution 2560 × 2160 pixels digitized at 16 bits. In this case, each camera independently recorded two-component data. One camera viewed the hemisphere to observe the shock motion while the other was located 80 mm upstream to simultaneously measure the incoming boundary layer. The hemisphere was imaged with a field of view similar to the first experiment, but a 400-mm lens (actually, a 200-mm lens plus a 2:1 teleconverter) and a shorter standoff distance allowed the boundary layer camera to obtain a much smaller field of view. Since the same laser sheet illuminated the flow seen by both cameras, the typical particle displacement was larger in the boundary layer, but this was easily accounted in the image interrogation. Images were analyzed using DaVis 8.1. Hemisphere images were interrogated as in the first experiment, whereas the boundary layer images used a first pass of a 128 × 128 pixel window with a constant initial offset corresponding to slightly less than the freestream velocity, followed by two iterations at 48 × 48 pixel using 4:1 elliptical Gaussian weighting to align with the dominant vertical velocity gradient. An overlap of 50% was again used and vector validation was similar.

Results

Approximately 2000 individual realizations have been acquired for the first, stereoscopic experiment; about 3400 realizations were acquired for the second, two-component experiment. These data quantities allowed sufficient statistical convergence for turbulence quantities and shock behavior. Results are given normalized to the hemisphere radius r_h and the freestream velocity U_∞. The origin of the coordinate axes was set to the upstream edge of the hemisphere at the wind tunnel floor.

The mean velocity field compiled from the 2000 stereoscopic realizations is given in Fig. 2. Vector fields shown in this figure are subsampled by two in the vertical direction and six in the streamwise direction, which improves the visual clarity of the results. The streamwise velocity u is emphasized by additionally showing it as a contour plot. The out-of-plane velocity component w was measured, but is effectively zero throughout the mean field. The mean flow can be observed to accelerate as it flows over the hemisphere, reaching a peak value just below u/U_∞=1.3. At this point, near the apex of the hemisphere, a shock wave forms and reduces the velocity. The

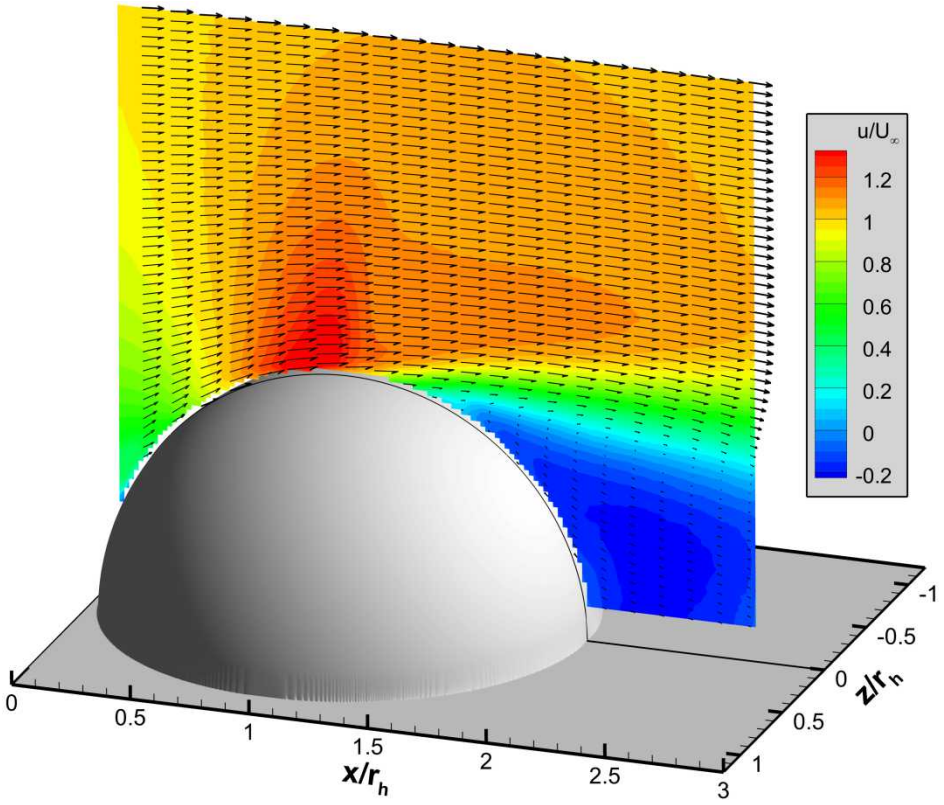

Fig. 2: Mean velocity field at M_∞=0.8. Vectors are subsampled by a factor of six in the streamwise direction and two in the vertical direction. Contours show the streamwise velocity magnitude.

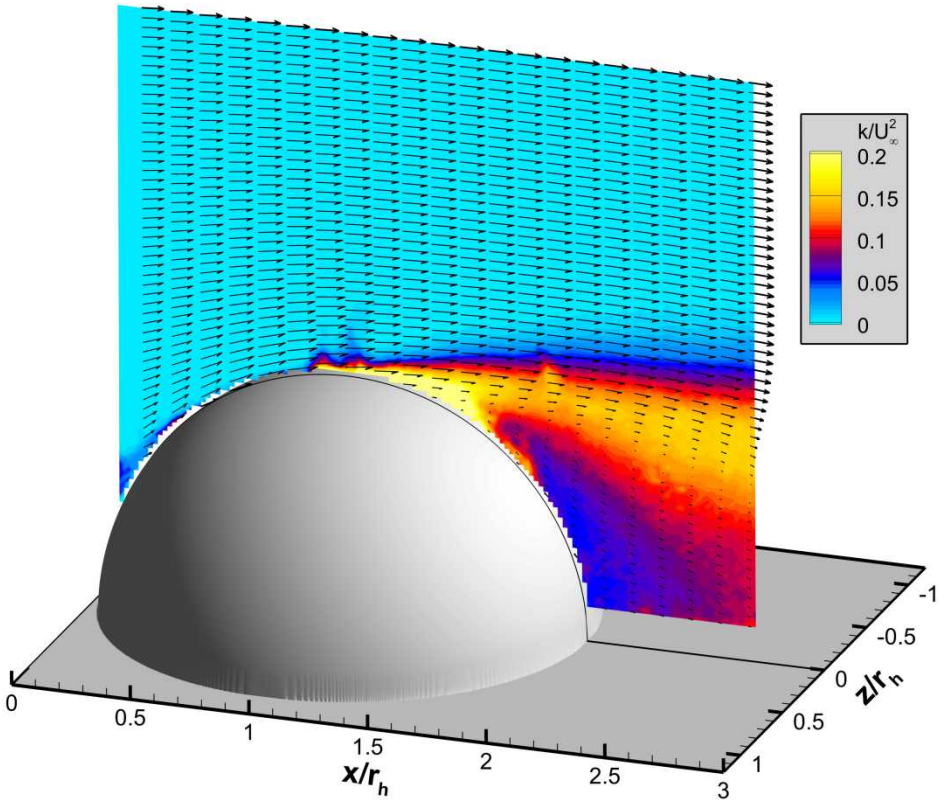

Fig. 3: Turbulent kinetic energy field at M_∞=0.8. The mean velocity vectors from Fig. 2 are overlaid on contours of k.

velocity drop does not appear abrupt because the shock wave is unsteady and its motion smears out the apparent velocity in the mean. The shock wave initiates separation and a strong shear layer and wake forms. A large, strong recirculation region is evident with reverse velocities exceeding u/U_∞=0.2 in magnitude. Reverse flow moves along the surface of the hemisphere back towards the separation point before recirculating to a positive velocity. The size of the separation region cannot be determined because it exceeds the field of view of the measurement, but it must be at least 1.8 r_h, or 5.1 δ since these are the distances to the edge of the images. Also, it can be seen in Fig. 2 that use of the acrylic hemisphere model allowed data to be acquired very near the surface, but data do not reach nearly as close to the wind tunnel wall where aluminum was used.

The turbulent activity of the flow can most readily be observed by examining the turbulent kinetic energy, shown in Fig. 3. Very little presence of the shock is detectable since the turbulence levels amplified by the shock primarily originate in the freestream and hence are far lower than those occurring in the wake. High levels of turbulence are visible just past the apex of the hemisphere where the shock resides and the onset of separation occurs, and remain elevated throughout the wake. The highest turbulence levels beyond the separation point occur fairly high in the wake where the shear layer is present, then diminish as the wall is approached. The high levels of turbulence seen at the leading edge of the hemisphere are not real, instead arising due to laser flare from the wind tunnel wall. Some interference also arises from the hemisphere itself as the laser burns the acrylic over time; this contributed to high levels of turbulence very near the hemisphere surface just past the point of separation.

Two examples of instantaneous realizations of the velocity field are given in Fig. 4. Here, vectors are sampled only 2 × 2 since greater spatial variation is seen in an instantaneous snapshot. As in Fig. 2, contours of u/U_∞ are given to reinforce the streamwise velocity. Contour levels are cut off below 0.8 for improved clarity of the vectors in the wake, but clearly reach much lower values as reverse flow is frequently seen. Both examples show several large turbulent eddies in the wake and the undulations of the shear layer take on different shape and height from the wall. When the data set as a whole is examined, the eddies tend to concentrate nearer the shear layer and reverse flow moves along the surface of the hemisphere back towards the separation point before recirculating to a positive velocity.

Also visible in the two samples shown in Fig. 4 is a differing shock position. Figure 4a shows the shock nearly normal and resting at x/r_h=1.07, slightly downstream of the apex of the hemisphere. Conversely, the shock foot in Fig. 4b sits at x/r_h=0.96, upstream of the hemisphere zenith, and has a distinct lean in the downstream direction. In the case of Fig. 4a, the maximum velocity prior to the shock is u/U_∞=1.42, whereas in Fig. 4b it is u/U_∞=1.36; this is indicative of the greater distance allowed for expansion of the flow when the shock is located farther downstream. An examination of a larger body of such instantaneous snapshots reveals a range of shock locations and shapes near the surface. This motion of the shock and variation in its shape is characteristic of a shock/boundary layer interaction as the turbulence in the incoming wake and/or the upstream boundary layer influences the instantaneous position.

To quantify the unsteady shock motion, the location of the shock can be found from each instantaneous velocity field and a probability density function of its position can be created. In the present case, this was accomplished by interpolating velocities onto a circular arc at some radius beyond the hemisphere surface and locating the point at which the velocity begins to rapidly fall. Ideally, the shock foot would be located by employing high-frequency pressure sensors in the surface of the hemisphere, but these were determined to be incompatible with the present experiment because of the need for the acrylic hemisphere to contain laser flare and the potential disturbance of a flat sensor face in a curved surface. However, velocity vectors near the surface clearly show the shock location and actually provide greater spatial resolution than a surface sensor could. Measurements reach to within about 1 mm, which captures the shock foot reasonably well. Velocity fields have been used as surrogates for shock foot position previously in shock/boundary layer experiments (e.g. [24, 25]).

Figure 5 shows the probability density function for the shock position at multiple heights above the hemisphere surface. These results are shown from the second, two-component PIV experiment because the signal-to-noise ratio was superior, but the equivalent data from the stereoscopic measurements are much the same. A height of r/r_h=1.05 is as close to the surface as measurements were found to be consistently effective with few spurious results, so this location acts as a surrogate for the shock foot position. This distribution in Fig. 5 shows that the shock foot typically sits just forward of the apex of the hemisphere, though it can move slightly onto the downstream slope. As the shock propagates away from the surface, it shifts downstream then gradually straightens, with the range of motion narrowing. Overall, the shock remains within a spread of about ±10 deg from the apex of the hemisphere. The few data points downstream of +10 deg probably are the result of spurious vectors, apparently as a result of laser flare as the surface becomes burned by the laser sheet, as these data points tended to occur later in the experiment.

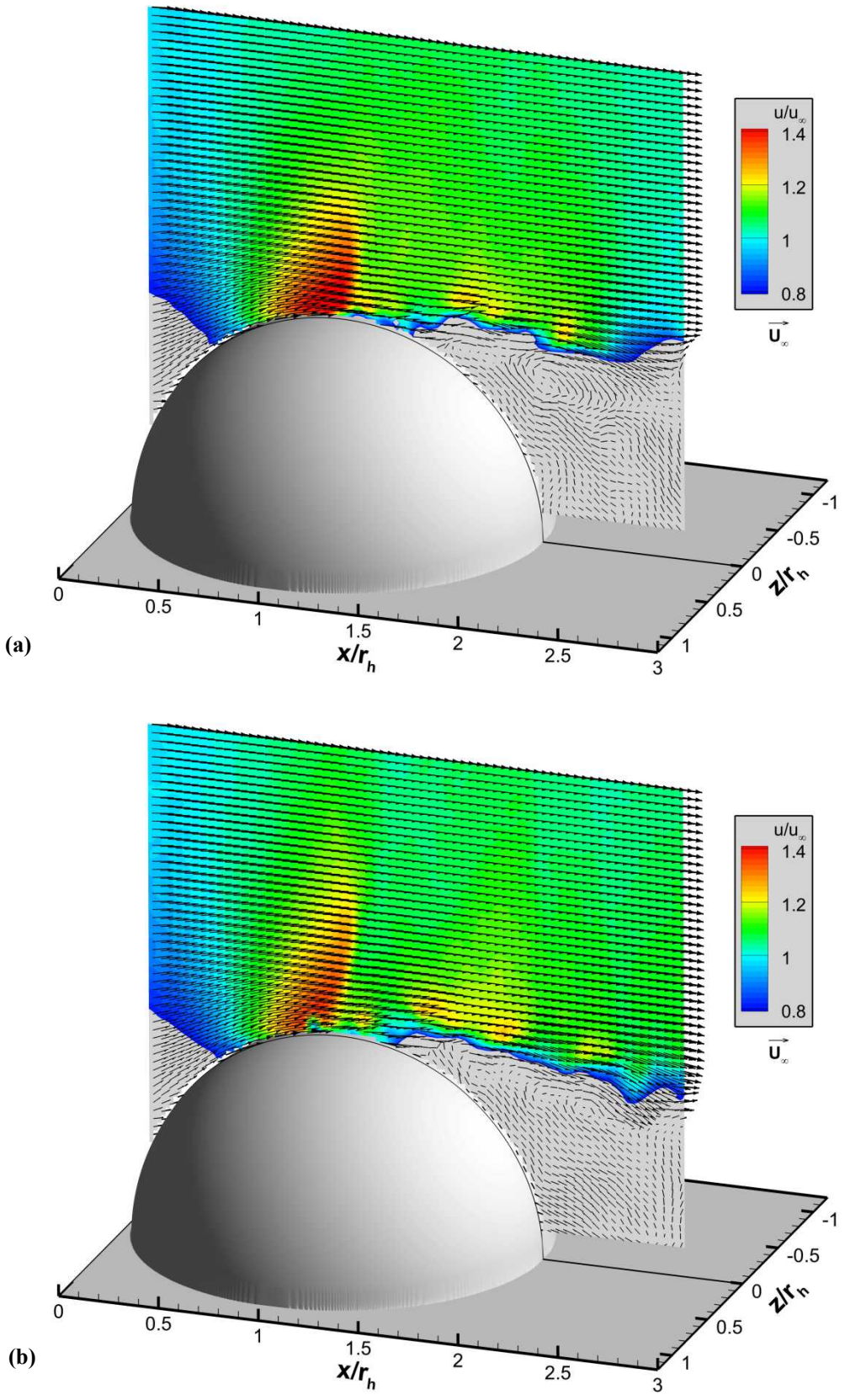

Fig. 4: Two sample instantaneous realizations of the flow at M_∞=0.8. Contour levels are cut off below 0.8 for improved clarity of the vectors in the wake. Vectors are subsampled 2 × 2.

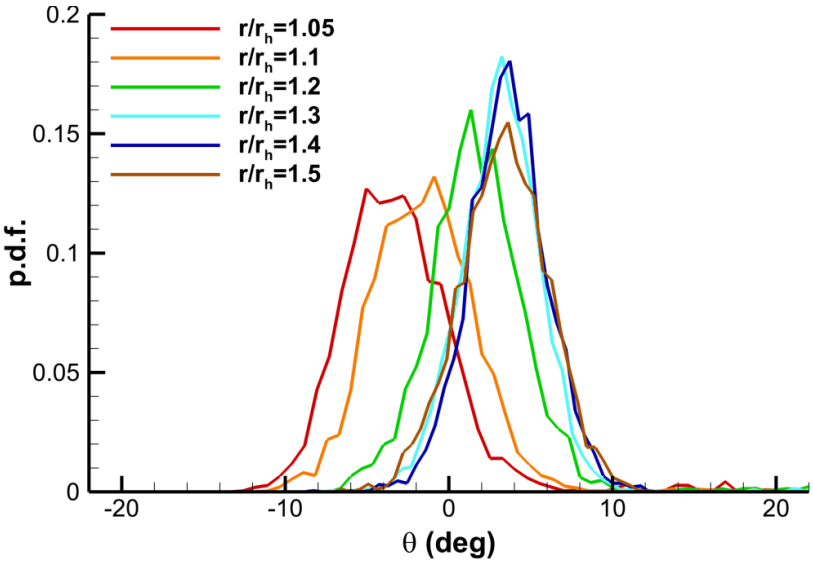

Fig. 5: Probability density functions of the shock location at several heights above the hemisphere surface, determined from the PIV data.

In an effort to locate a correlation between the wake structure and the shock motion, conditional averages were generated based on the shock foot position as determined by the r/r_h=1.05 data. Two conditional vector fields were created, one representing when the shock foot lay more than one standard deviation σ_r upstream of the mean point, and a second for the shock foot more than one standard deviation downstream. These results are given in Fig. 6. Here, the contours represent the total velocity magnitude, u_t, rather than just the streamwise component. Vectors again are subsampled 6 × 2 and are removed at velocities above 0.6 U_∞ to focus upon the wake. Data are given from the stereoscopic experiment for access to the third velocity component, although the results were found identical when the later two-component data were employed.

The separation region appears to possess the same structure in both the shock-upstream and shock-downstream cases of Fig. 6, but it is located at differing positions along the hemisphere surface. More significantly, the magnitudes of the reverse velocities are greater in the upstream shock case, suggesting that stronger reverse flow adjusts the shock to an upstream location. However, it is impossible to differentiate cause and effect since the shock position is recorded simultaneously with the wake velocities. Even though the entire separation region is not visualized, it is possible to estimate that it is larger in the shock-upstream case than the shock-downstream case; the reversal of velocities at the downstream end of the separation region is visible in the shock-downstream case but not the shock-upstream case.

To better appreciate the correlation between the shock position and the reverse velocity magnitude in the recirculation region, probability density functions of the velocity tangential to the hemisphere surface are given in Fig. 7. This tangential velocity, u_θ, was found at a height of r/r_h=1.05 between the azimuthal angles of 30 deg and 40 deg, which is where the strongest influence of the wake velocity is observed in Fig. 6. Figure 7 displays three curves, one for the shock-upstream case, one for the shock-downstream case, and a third for a shock-middle case in which the shock lay positioned between -0.5 σ_r and +0.5 σ_r, where σ_r is the standard deviation of the shock foot position.

Figure 7 provides a more quantitative interpretation of the conditional vector fields of Fig. 6. When the shock is positioned in an upstream location, reverse velocities in the wake along the surface of the hemisphere tend to be large, whereas shocks in a downstream position tend to be associated with weaker reverse velocities or positive velocities. When the shock is near its mean position, the tangential velocity distribution is roughly halfway between the shock-upstream and shock-downstream cases. Also, it is evident that the tail of the distribution grows longer as the shock is located farther downstream. Despite having obtained three distinct p.d.f.'s, all three distributions show significant overlap. This indicates that the correlation is imperfect, for which several explanations are possible. The shock position and wake velocities are measured simultaneously, whereas some time lag must actually occur before one influences the other; therefore, the p.d.f.'s are not measured at the time of the strongest correlation. The shock may be additionally influenced by velocities at different heights above the surface or at different points in the wake. The reverse velocities in the wake may actually have a primary correlation to the shock motion and its correlation

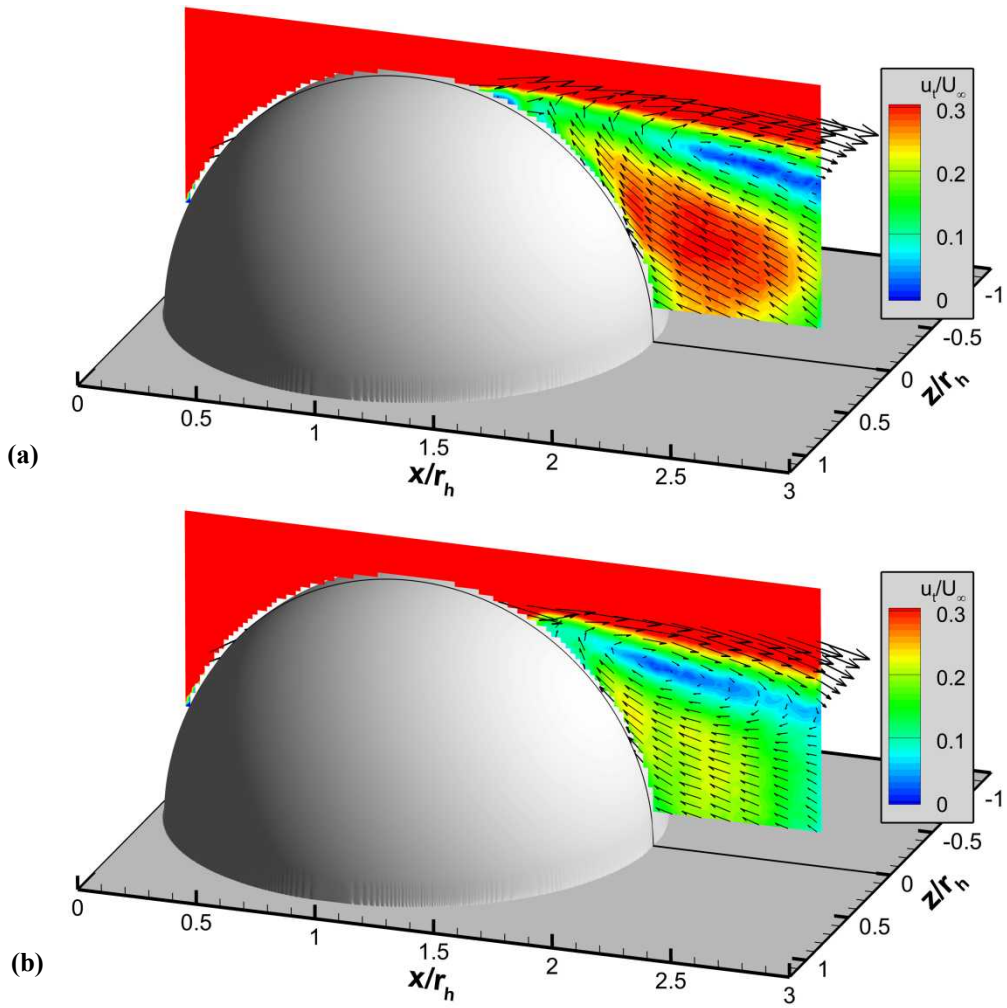

Fig. 6: Conditional averages of the wake for (a) shock upstream and (b) shock downstream cases; contours are given for the total velocity magnitude.

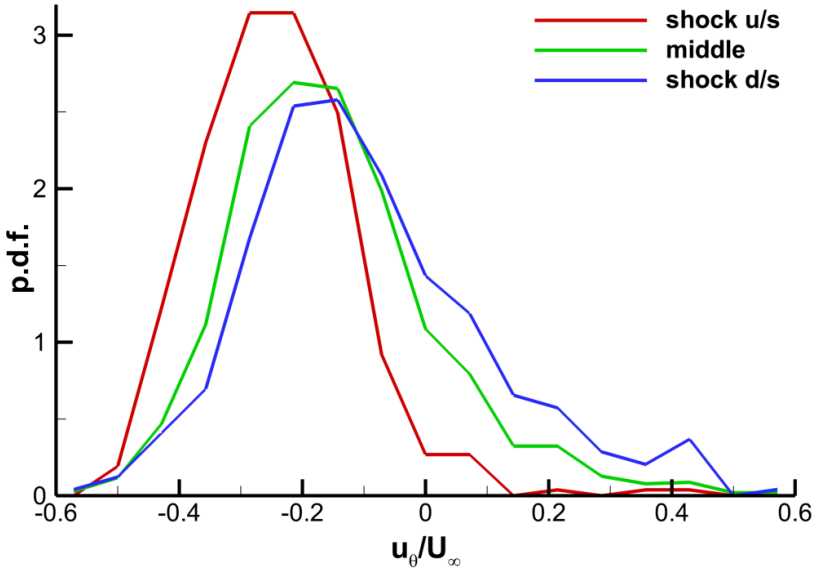

Fig. 7: Probability density functions of the tangential velocity in the wake near the hemisphere surface, conditioned upon the shock foot location.

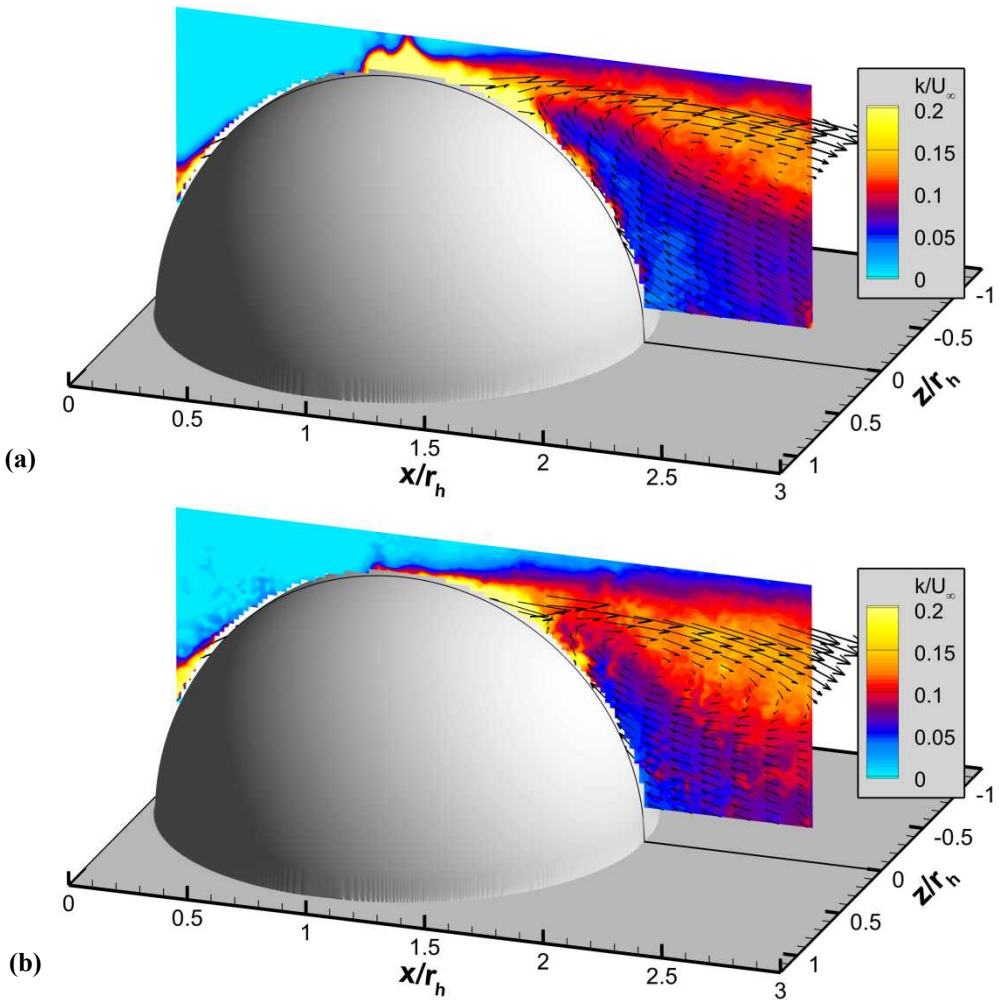

Fig. 8: Conditional turbulent kinetic energy fields of the wake for (a) shock upstream and (b) shock downstream cases. The mean velocity vectors from Fig. 6 are overlaid on contours of *k*.

to the shock position is residual from such a true correlation. Or, the effect of the recirculation velocity is not the sole mechanism for shock motion, and the shock position is influenced by additional flow field parameters such as the incoming wall boundary layer.

Conditional turbulent kinetic energy fields were generated as well in the same fashion, and they are shown in Fig. 8. The data are not well converged since the quantity of vector fields contained in each sample is about 300, which is a relatively small sample for turbulence statistics. Still, it is possible to recognize that the structure of the turbulence fields remains much the same but relocates as the shear layer and recirculation region changes with shock position. No evidence can be seen for a change in turbulence intensity with shock position. A greater extent of elevated turbulence levels is apparent in the shock-downstream case, but this likely is an effect of the smaller recirculation region drawing more of the shear layer into the field of view.

Figures 6 and 7 establish a correlation between the shock position and the velocities within the separation region, but this does not rule out that an additional correlation may exist between the shock position and the incoming boundary layer. The simultaneous measurements of the incoming boundary layer from the second, two-component experiment were designed to address this question, at least for low-frequency influences that can be captured in simultaneous exposures. Similar to Fig. 6, conditional velocity profiles of the boundary layer were generated 65 mm upstream of the hemisphere leading edge based upon shock upstream and shock downstream cases, which are given in Fig. 9 along with an average of all boundary layer data. No difference can be identified.

Though the boundary layer and shock position are recorded simultaneously, the distance traveled between these points corresponds to roughly 3 kHz. A direct influence of the upstream boundary layer upon the shock position,

were it to exist, should be detectable if the frequency character of the shock motion is much lower than this 3 kHz value. The historical database suggests that low-frequency large-scale shock motion can be expected approximately two orders of magnitude lower than the characteristic frequency $f=U_\infty/\delta$ [2, 3, 6], which in the present case is about 20 kHz. Therefore the expected dominant frequency of large-scale shock motion is approximately 200 Hz and measurement of it should be minimally degraded by the 3 kHz response time of the measurement. This suggests that the absence of a correlation in Fig. 9 is not due to a measurement limitation.

If the incoming boundary layer does not directly influence the shock motion, it may still correlate with the shock position if it influences the shear layer instability at separation. This could cause a velocity fluctuation in the wake that recirculates back to the shock wave and affects it from downstream. Such a process would have a longer time lag and be difficult to detect using the present simultaneous measurements, but may have a more direct correlation than between the boundary layer and the shock position. Nevertheless, a correlation was sought by again generating conditional velocity profiles of the incoming boundary layer, but instead provisioned on the tangential velocity in the wake as in Fig. 7. Conditional profiles were created for two cases, one in which the tangential wake velocity was at least one standard deviation less than the mean, and another in which the tangential wake velocity was at least one standard deviation greater than the mean. As in Fig. 9, no significant difference was found between these two velocity profiles and a mean profile. The figure is omitted since it is materially indistinguishable from Fig. 9.

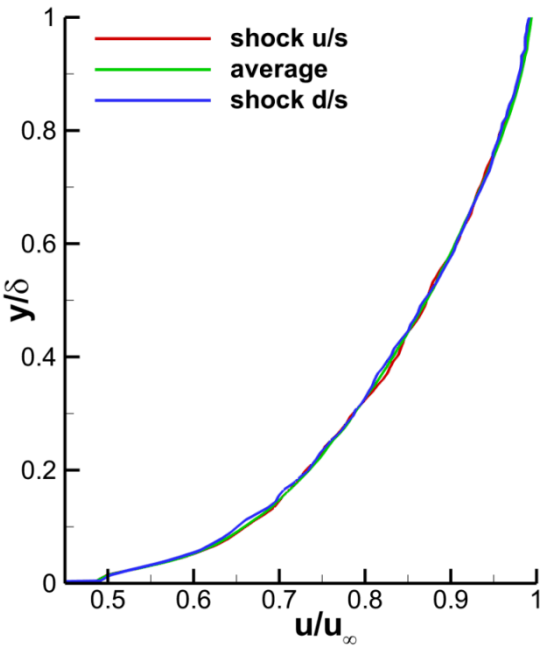

Fig. 9: Conditional velocity profiles of the incoming boundary layer based on different shock positions; acquired 65 mm upstream of the hemisphere.

Discussion

For many years, the shock/boundary-layer interaction community has debated whether the shock motion is caused by turbulent fluctuations in the incoming boundary layer or by turbulent fluctuations in the downstream recirculation region. The number of studies weighing in on this matter is much too voluminous to compile here, but good summaries of the situation are provided by Dolling [3] and Clemens and Narayamaswamy [6]. Recently, a wide-ranging reassessment of data in the open literature by Clemens and Narayamaswamy [6] has begun to offer a reconciliation of the two views that explains the source of the shock motion contingent upon specific flow conditions. A narrower examination of incident shock experiments by Souverein et al [26] is supportive of this perspective. Dussauge and Piponniau [27] offered similar views as well.

These careful assessments of the data indicate that both sources of shock motion are present in shock/boundary-layer interactions, but which one emerges as the dominant mechanism is a result of the degree of separation found in the wake of the shock. For incipient separation or small separation regions, the upstream boundary layer mechanism is dominant. For strongly separated flows, the downstream recirculation region mechanism is dominant.

By the criteria of [6], the present flow clearly would be considered to be strongly separated. They distinguish a strongly separated flow from a weakly separated flow by the size of the recirculation region and the presence of mean reverse flow within it. Their analysis indicates that an approximate division between weakly and strongly separated flows can be noted when the length of the separated region exceeds about 2 – 3 boundary layer thicknesses. In the present case, the exact length of the separated region cannot be determined because it extends beyond the downstream limit of the measurement. However, the streamwise distance from the mean shock location to the edge of the field of view is 1.8 r_h, or 5.1 δ; Fig. 2 suggests the length of the separation region is considerably longer than this. Moreover, a reverse velocity is present in the mean velocity field, with a maximum magnitude (tangent to the hemisphere surface) of about 0.2 U_∞. Clearly, this is a strongly separated flow. Accordingly, it would be expected that the downstream mechanism will be dominant as a source of shock motion.

The present analysis has shown a distinct correlation between the reverse velocities in the recirculation region and shock motion, whereas no correlation is observed with the incoming boundary layer velocity profile. For a strongly separated flow, this is consistent with the theory expressed by Clemens and Narayamaswamy [6] and Souverein et al [26]. It further appears from Fig. 6 that the recirculation region is smaller when the shock is located farther downstream. This would be consistent with the behavior observed over compression corners or other obstacles [3, 6] as well as incident shocks [28]. Because measurements of the separation region were simultaneous with those of the shock location, no comment may be made whether reverse velocity fluctuations precede the shock motion, and therefore regarding cause and effect.

As pointed out by Clemens and Narayamaswamy [6], the dominance of the downstream mechanism for strongly separated flows does not preclude the additional existence of an influence of the upstream boundary layer on the shear layer instability and hence the recirculation region structure. Such a correlation would be more likely to occur at higher frequencies associated with boundary layer and shear layer turbulence, which would make it more difficult to detect in the present work. However, Dussauge and Piponniau [27] found that while the three-dimensional structure of the recirculation region did indeed respond to changes in the incoming boundary layer, the motion of the shock wave did not. Piponniau et al [28] found a very small correlation, not exceeding the measurement uncertainty. Clemens and Narayamaswamy [6] further suggest that the larger the separation region, the less it is dependent upon the upstream boundary layer.

As a final note, all the data examined by Clemens and Narayamaswamy [6] and Souverein et al [26] to deduce a mechanism for the shock motion incorporating both upstream and downstream influences were supersonic. The current work appears to be the first to offer measurements of shock motion in transonic flow past an obstacle, yet the results are fully consistent with the data at higher Mach numbers. However, it is possible that the present transonic case is subject to an additional downstream mechanism in which acoustic waves propagate upstream outside the separation region to influence the shock motion. Lee [7] describes such an effect in shock motion over transonic airfoils.

Conclusions

Particle image velocimetry measurements have been conducted for a Mach 0.8 flow over a wall-mounted hemisphere. The resulting velocity fields reveal the turbulent structure of the wake and can be used to determine the instantaneous shock location. The flow clearly is strongly separated, with a mean recirculation length exceeding five boundary layer thicknesses and a mean reverse velocity magnitude of 0.2 U_∞. The highest levels of turbulence are found in the shear layer originating at the separation point, but elevated turbulence is present in the recirculation region as well. Considerable undulation of the shear layer is observed. The shock foot was found to move within a range of about ±10 deg from the apex of the hemisphere, but typically it sits just forward of the apex. As the shock propagates away from the surface, it shifts downstream then gradually straightens, with the range of motion narrowing.

Conditional averages based upon the shock foot location were used to detect the source of the unsteady shock motion. The current measurements show that the position of the transonic separation shock on the hemisphere surface is located upstream when the reverse velocities in the recirculation region are strong and is located downstream when they are weaker. The recirculation region appears smaller when the shock is located farther downstream. No correlation was detected between the incoming boundary layer and the shock position. Nor was a correlation found between the incoming boundary layer and the wake recirculation velocities. These observations are consistent with recent studies concluding that for large strong separation regions, the dominant mechanism is the instability of the separated flow rather than a direct influence of the incoming boundary layer. However, it is possible that the upstream boundary layer influences the shock position by affecting the shear layer instability at separation, which would not be captured by the present experiment if it occurs at high frequencies or long response times.

References

[1] Gordeyev, S., and Jumper, E., "Fluid Dynamics and Aero-Optics of Turrets," *Progress in Aerospace Sciences*, Vol. 46, No. 8, 2010, pp. 388-400.

[2] Smits, A. J., and Dussauge, J.-P., *Turbulent Shear Layers in Supersonic Flow*, 2nd ed., Springer, New York, 2006, pp. 319-363.

[3] Dolling, D. S., "Fifty Years of Shock-Wave/Boundary-Layer Interaction Research: What Next?", *AIAA Journal*, Vol. 39, No. 8, 2001, pp. 1517-1531.

[4] Delery, J. M., "Shock Wave/Turbulent Boundary Layer Interaction and its Control," *Progress in Aerospace Sciences*, Vol. 22, No. 4, 1985, pp. 209-280.

[5] Knight, D., Yan, H., Panaras, A. G., and Zheltovodov, A., "Advances in CFD Prediction of Shock Wave Turbulent Boundary Layer Interaction," *Progress in Aerospace Sciences*, Vol. 39, No. 2-3, 2003, pp. 121-184.
[6] Clemens, N. T., and Narayanaswamy, V., "Shock/Turbulent Boundary Layer Interactions: Review of Recent Work on Sources of Unsteadiness," AIAA Paper 2009-3710, June 2009.
[7] Lee, B. H. K., "Self-Sustained Shock Oscillations on Airfoils at Transonic Speeds," *Progress in Aerospace Sciences*, Vol. 32, No. 2, 2001, pp. 147-196.
[8] Delery, J. M., "Experimental Investigation of Turbulence Properties in Transonic Shock/Boundary-Layer Interactions," *AIAA Journal*, Vol. 21, No. 2, 1983, pp. 180-185.
[9] Bachalo, W. D., and Johnson, D. A., "Transonic, Turbulent Boundary-Layer Separation Generated on an Axisymmetric Flow Model," *AIAA Journal*, Vol. 24, No. 3, 1986, pp. 437-443.
[10] Liu, X., and Squire, L. C., "An Investigation of Shock/Boundary-Layer Interactions on Curved Surfaces at Transonic Speeds," *Journal of Fluid Mechanics*, Vol. 187, 1988, pp. 467-486.
[11] Sandham, N. D., Yao, Y. F., and Lawal, A. A., "Large-Eddy Simulation of Transonic Turbulent Flow over a Bump," *International Journal of Heat and Fluid Flow*, Vol. 24, No. 4, 2003, pp. 584-595.
[12] Barakos, G., Huang, J.C., Benard, E., Yapalparvi, R., and Raghunathan, S., "Investigation of Transonic Flow over a Bump: Base Flow and Control," AIAA Paper 2008-0357, January 2008.
[13] Bodin, O., and Fuchs, L., "Shock Unsteadiness and Shock Induced Separation at Transonic Flow over a Bump," AIAA Paper 2008-4174, June 2008.
[14] Ogawa, H., Babinsky, H., Patzold, M., and Lutz, T., "Shock-Wave/Boundary-Layer Interaction Control Using Three-Dimensional Bumps for Transonic Wings," *AIAA Journal*, Vol. 46, No. 6, pp. 1442-1452, 2002.
[15] Wollblad, C., Davidson, L., and Eriksson, L. E., "Investigation of Large Scale Shock Movement in Transonic Flow," *International Journal of Heat and Fluid Flow*, Vol. 31, No. 4, pp. 528-535, 2010.
[16] Reid, J. Z., Lynch, K. P., and Thurow, B. S., "Density Measurements of a High-Speed, Compressible Flow Field Using Acetone Planar Laser Induced Fluorescence (PLIF)," AIAA Paper 2011-0987, January 2011.
[17] Fang, S., Disotell, K. J., Long, S. R., Gregory, J. W., Semmelmeyer, F. C., and Guyton, R. W., "Application of Fast-Responding Pressure-Sensitive Paint to a Hemispherical Dome in Unsteady Transonic Flow," *Experiments in Fluids*, Vol. 50, No. 6, pp. 1495-1505, 2011.
[18] Gordeyev, S., Hayden, T. E., and Jumper, E. J., "Aero-Optical and Flow Measurements Over a Flat-Windowed Turret," *AIAA Journal*, Vol. 45, No. 2, 2007, pp. 347-357.
[19] Gordeyev, S., Post, M. L., McLaughlin, T., Ceniceros, J., and Jumper, E. J., "Aero-Optical Environment Around a Conformal-Window Turret," *AIAA Journal*, Vol. 45, No. 7, 2007, pp. 1514-1524.
[20] Cress, J. A., Gordeyev, S., Jumper, E. J., Ng, T. T., and Cain, A. B., "Similarities and Differences in Aero-Optical Structure over Cylindrical and Hemispherical Turrets with a Flat Window," AIAA Paper 2007-0326, January, 2007.
[21] Perohit, S. C., Shang, J. S., and Hankey Jr., W. L., "Effect of Suction on the Wake Structure of a Three-Dimensional Turret," AIAA Paper 1983-1738, July 1983.
[22] Vukasinovic, B., and Glezer, A., "Control of Separating Flow over a Turret," AIAA Paper 2007-4506, June 2007.
[23] Vukasinovic, B., Glezer, A., Gordeyev, S., Jumper, E., and Kibens, V., "Hybrid Control of a Turret Wake," *AIAA Journal*, Vol. 49, No. 6, 2011, pp. 1240-1255.
[24] Ganapathisubramani, B., Clemens, N. T., and Dolling, D. S., "Effects of Upstream Boundary Layer on the Unsteadiness of Shock-Induced Separation," *Journal of Fluid Mechanics*, Vol. 585, 2007, pp. 369-394.
[25] Humble, R. A., Elsinga, G. E., Scarano, F., and van Oudheusden, B. W., "Three-Dimensional Instantaneous Structure of a Shock Wave/Turbulent Boundary Layer Interaction," *Journal of Fluid Mechanics*, Vol. 622, 2009, pp. 33-62.
[26] Souverein, L. J., Dupont, P., Debieve, J.-F., Dussauge, J.-P., van Oudheusden, B. W., and Scarano, F., "Effect of Interaction Strength on Unsteadiness in Turbulent Shock-Wave-Induced Separations," *AIAA Journal*, Vol. 48, No. 7, 2010, pp. 1480-1493.
[27] Dussauge, J.-P., and Piponniau, S., "Shock/Boundary-Layer Interactions: Possible Sources of Unsteadiness," *Journal of Fluids and Structures*, Vol. 24, No. 8, 2008, pp. 1166-1175.
[28] Piponniau, S., Dussauge, J. P., Debieve, J. F., and Dupont, P., "A Simple Model for Low-Frequency Unsteadiness in Shock-Induced Separation," *Journal of Fluid Mechanics*, Vol. 629, 2009, pp. 87-108.